

Optimal Machine Intelligence Near the Edge of Chaos

Ling Feng^{1,2}, Choy Heng Lai^{2,3,4}

¹Institute of High Performance Computing, A*STAR, 138632 Singapore.

²Department of Physics, National University of Singapore, 117551 Singapore.

³Centre for Quantum Technologies, National University of Singapore, 117543 Singapore.

⁴NUS Graduate School for Integrative Sciences and Engineering, 119077 Singapore.

It has long been suggested that living systems, in particular the brain, may operate near some critical point. How about machines? Through dynamical stability analysis on various computer vision models, we find direct evidence that optimal deep neural network performance occur near the transition point separating stable and chaotic attractors. In fact modern neural network architectures push the model closer to this edge of chaos during the training process. Our dissection into their fully connected layers reveals that they achieve the stability transition through self-adjusting an oscillation-diffusion process embedded in the weights. Further analogy to the logistic map leads us to believe that the optimality near the edge of chaos is a consequence of maximal diversity of stable states, which maximize the *effective* expressivity.

There has been abundant suggestive evidence that many natural systems operate around the critical point between order and disorder (*1*). In particular the brain activities exhibit various spatio-temporal patterns of scale-invariance, which resemble that of critical phase transitions in statistical mechanics (*2, 3*). However, direct evidence of criticality on these systems are lacking due to the practical limitations to measure their exact microscopic dynamics to validate the

claim. On the theoretical front, self-organized criticality (4) was proposed to explain the prevalence of scale-invariance in nature. Certain complexity measures are shown to be maximized at the edge of chaos of dynamical systems (5). Some simple computer models have been able to demonstrate that certain non-linear systems at criticality possess maximal adaptivity and information processing capability, leading to the hypothesis that living systems optimize themselves towards the critical state to maximize adaptivity and survival (6). Early neural networks models have been able to show clear correlation between edge of chaos and computational power (7, 8). Yet, direct links between this hypothesis and observed data have not yet been established.

The recent rise of deep neural networks has brought this idea of criticality to the attention of computer scientists. Mean-field analysis (9) on forward and backward propagation indicates that optimal parameter initialization needs to be at the edge of chaos, such that exploding or vanishing signals can be avoided to achieve faster training (10, 11). This principle coincides with the empirical pattern in the brain dynamics, that brain neural signals propagate at a branching ratio of 1, i.e. neither vanishing nor exploding (12). With computer simulations, this critical branching mechanism is shown to maximize number of metastable states, which is proposed as the possible reason for the observed criticality (13).

Deep neural network models, especially in computer vision, have evolved to the performance comparable to human's. Their complete tractability and controllability at the lowest microscopic level allow us to find more conclusive evidence on the existence of edge of chaos, as well as the underlying mechanism of how they reach this state. For the best performing neural network models used in computer vision, there are several different architectures, initialization schemes, optimisers and regularization techniques. We first begin with the simple architecture of fully connected feed-forward networks illustrated in figure 1A, also known as multi-layer perception (MLP), trained using the widely adopted 'adam' optimizer (14).

Neural network is effectively an operator that outputs values based on the inputs. Theoret-

ically its stability property can be studied analytically. But given the high dimensionality and non-linearity of the models, it is usually rather difficult. Yet numerically, it is possible to accurately analyze its stability through simulated dynamic evolution by the operator on arbitrary inputs. The only constraint is that the operator’s input and output must have the same dimension. Since in computer vision tasks the input (image) and output (classes) are almost always different, we customized the various network architectures such that the last non-linear layer before the output has the same dimension as the input image. Such design has impacts on the final accuracy of the models, but not significantly as the model architectures are robust against various modifications (tables 1-3). Next we extract the bulk of the network by removing the final output layer (figure 1A), and repeatedly apply it for 200 iterations on each of the 10,000 test images in the Fashion MNIST datasets¹, as well as a noisy version from each of them. Figure 1B shows that before any training at epoch 0, the operator extracted from the MLP model (2 hidden layers) is in the stable phase, as the both images evolves towards the trivial stable equilibrium point of 0. This is in line the with the results from mean-field analysis (9). Later in the training at epoch 12, the difference between the two images grows with more iterations, eventually diverging to infinity. Hence the network at epoch 12 is in the unstable phase. Looking at the size of the 2 images in terms of their Euclidean lengths in figure 1C, the dynamical operator evolves from the stable phase at epoch 0, to a chaotic attractor phase in epoch 9, before reaching the unstable phase of epoch 12. Such evolution shares striking resemblance to the phase transition behaviors in the logistic map (15). A single metric to characterize stability is the maximal Lyapunov exponent γ , which is the dynamical system’s exponential rate of path divergence under small perturbations (16) (Methods section). We find that as the training proceeds, the most optimal model (having lowest test loss function) is at $\gamma \approx 0$ (figure 1D), i.e. at the edge of stability.

¹<https://github.com/zalandoresearch/fashion-mnist>

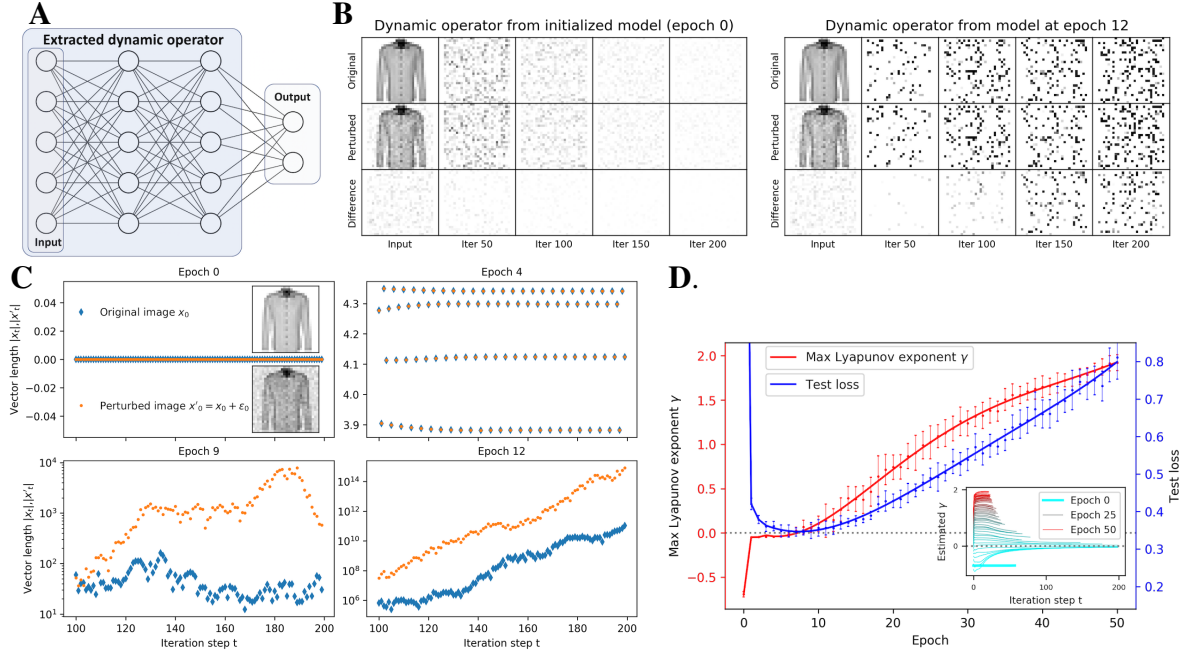


Figure 1: **Stability analysis of 2-hidden-layer fully connected neural network.** Training and testing is carried out on Fashion MNIST dataset. (A). Illustration of dynamic operator extraction from the neural network by removing the output layer, while designing hidden layers to have same dimension of 784 as input. (B). At different training stages (epoch 0 and 12), the extracted dynamic operator is iteratively applied on an input data (shirt) as well as its perturbed counterpart (adding a small Gaussian noise ϵ). Epoch 0 is a stable operator since the original and perturbed image become the same after 200 iterations, and epoch 12's model is unstable as the difference grows. The average rate that their difference grows/diminishes is used to estimate the maximum Lyapunov exponent γ . (C). Stability of the length $\|x_t\|$ of the same image and that of its perturbed counterpart $\|x'_t\| = \|x_0 + \epsilon\|$. At the beginning (epoch 0) the network operator has only one trivial stable point of $q^* = 0$, which then becomes a periodic cycle of 4 values at epoch 4, similar to the logistic map before the first onset to chaos. It then evolves to a chaotic attractor phase at epoch 9 with no clear correlation between $\|x_t\|$ and $\|x'_t\|$. Eventually at epoch 12 the system becomes unstable and diverges, similar to the logistic map at $r > 4$. (D). The value γ is estimated from the asymptotic rate of divergence/convergence of path separation $\|x_t - x'_t\|$ within 200 steps of iteration of the neural network dynamic operator, averaged over the 10000 testing images as shown in the inset (γ values at some epochs are not computable beyond certain t due to numerical limit.). The network evolves from being stable at $\gamma < 0$ (under-fitting) to unstable at $\gamma > 0$ (over-fitting). The optimal model (lowest test loss) is near epoch 8 when the model is at the edge of stability $\gamma \approx 0$. The error bars represent the standard error of 10 independent experiments.

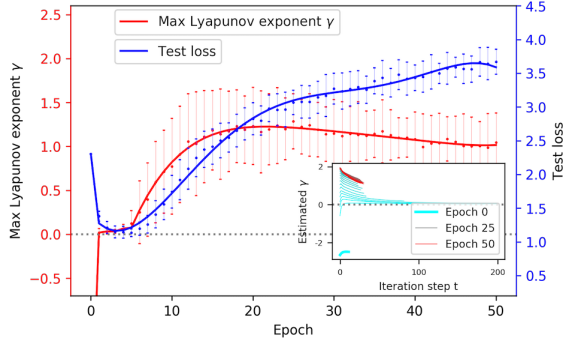
Repeating the same analysis on the more advanced architecture of convolutional networks (CNN), the same optimality at the edge of chaos is found (figure 2A). Furthermore, with the popular model regularization technique dropout (17) implemented, the same CNN model stays close the edge of criticality at $\gamma \approx 0$ as it becomes more optimal (figure 2B). We further carry out the stability analysis on the modern architectures Residual network (18) and DenseNet (19), with additional techniques including data augmentation, batch normalization (20) and better initializations in figure 2C,D. Both architectures exhibit the same edge of chaos behaviors, even if the model starts from the unstable phase for ResNet due to its different initialization. In both cases model optimality is closely associated with the closeness to the edge of chaos inferred from γ , i.e. more optimal model is closer to the edge between stable and chaotic attractors. We have validated this result more extensively on various versions of these network architectures, for longer training epochs as shown in figure 6-8.

To further investigate the underlying nature of the phase transitions from order to disorder, we examine the evolution of fully connected layers inside the various network architectures. For architectures other than MLP, we design this fully connected layer to have the same dimension as its previous layer to draw comparison with MLP, and place it right before the output layer, which is the common position for fully connected layers. Mathematically this operator is:

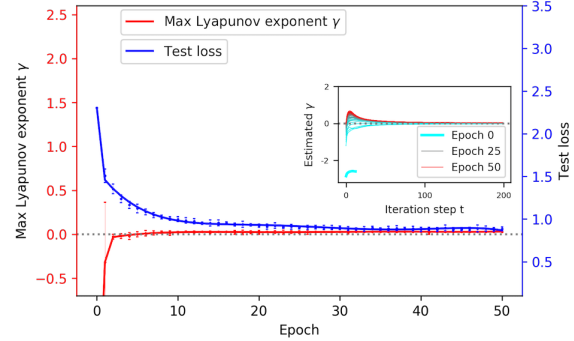
$$f_{dense}(\mathbf{x}_{t+1}) = \phi_{ReLU}(\mathbf{W}\mathbf{x}_t + \mathbf{b}), \quad (1)$$

where \mathbf{W} is a square matrix and ϕ_{ReLU} is rectified linear unit commonly used in computer vision. The dominant properties of \mathbf{W} can be analyzed through the properties of its eigenvalues (21). For all of the networks studied, the eigenvalues of \mathbf{W} have identical evolution patterns: before training they are uniformly distributed within a unit circle of radius 1 centered around 0 on the complex plane, following the known results from random matrix theory (22); later a dominant real eigenvalue λ_0 emerges and becomes more negative, and the distribution of other

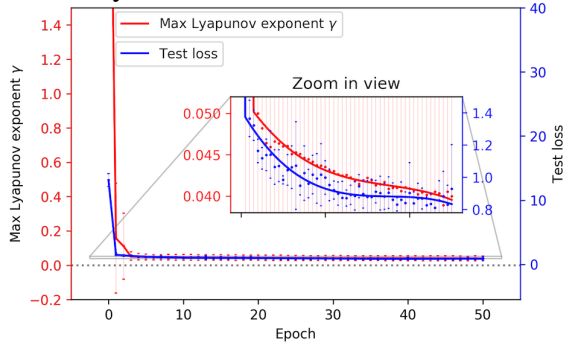
A. 5-layer Convolutional network (CNN)



B. 5-layer CNN with dropout



C. 20-layer Residual network



D. 17-layer DenseNet

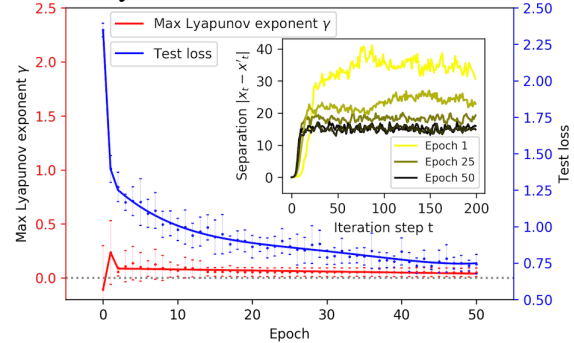


Figure 2: Maximal Lyapunov exponent γ in various neural network architectures. The experiments are carried out on the Cifar10 image dataset. (A). The plain convolutional network has similar results as fully connected network in Fig. 1(D), with the optimal model appearing at $\gamma \approx 0$. (B). With the popular regularization technique *dropout* to prevent overfitting, the network remains close to the edge of stability, i.e. $\gamma \approx 0$. Advanced architectures like residual network (C) and dense convolutional network (D) with advanced modeling techniques including dropout (only on DenseNet), batch normalization and data augmentation. Both evolve towards $\gamma = 0$ with more training epochs as models become more optimal (lower test loss, inset in (C)). Note that although $\gamma > 0$ at later epochs for (C) and (D), it does not mean the models are in the unstable phase. As seen in the inset of (D), the path separation $\|x_t - x'_t\|$ used to estimate γ does not converge to 0 nor diverge, but fluctuate in a chaotic attractor, similar to the logistic map chaotic attractor after the 1st onset to chaos at $r \approx 3.569$. Furthermore, more training epochs shrink the size of the chaotic attractor (smaller $\|x_t - x'_t\|$ range), pushing the model closer to the edge separating order and chaos.

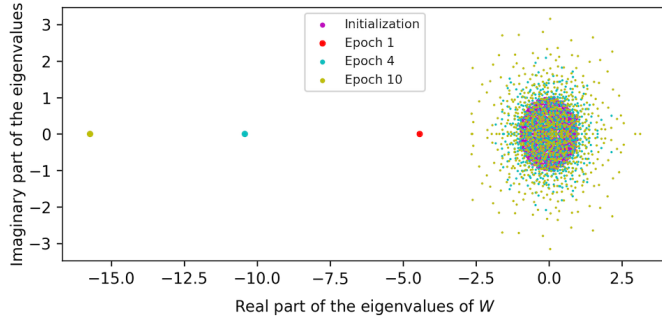
complex eigenvalues centered around 0 expands continuously (figure 3A and figure 9-14). The dominant component \mathbf{W}_0 in the matrix associated with the dominant eigenvalue λ_0 creates a negative feedback mechanism together with the non-linear activation ϕ_{ReLU} . Hence the projection r_0 of \mathbf{x}_t on this dominant eigenvector \mathbf{v}_0 oscillates around some equilibrium values shown in figure 3B. The combined action from the cluster of eigenvalues centered around 0 is similar to a diffusion process. It expands the length q_t of \mathbf{x}_t and becomes stronger with more training. The complex dynamics between these two components drive the system from the stable phase to the chaotic attractor phase, then unstable phase as demonstrated in figure 3C. The phase transition mechanisms behind the convolutional layers and skip connections are more complex to analyse, and we leave it for future studies.

Therefore, by reducing the high dimensionality of the fully connected layer to 2 major components, we observe a remarkable resemblance in figure 3 to the logistic map (15): $x_{t+1} = g_r(x_t) = rx_t(1 - x_t)$. Indeed many of the above features during an order-to-chaos transition are common in different types of non-linear systems (23). Hence to gain theoretical clarity on why optimal models are near the edge of chaos, we leverage on the existing knowledge from the logistic map, also to avoid the difficulty dealing with the high dimensionality and complexity of the neural networks. To introduce high non-linearity to mimic deep neural networks, we construct a pseudo neural network that consists of 100 layers of logistic map function, i.e.

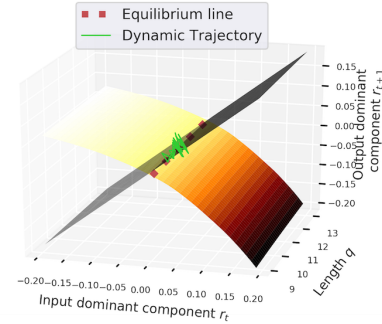
$$x^{out} := x^{100} = \underbrace{g_r \circ \dots \circ g_r}_{100 \text{ times}}(x^0) := f_r(x^{in}). \quad (2)$$

This network has only 1 parameter $r \in (0, 1)$, while both input and output are of dimension 1. As r increases from the stable phase $r = 3.4$ to the first onset to chaos at $r \approx 3.57$, the output x^{out} occupies more (almost) discrete states (figure 4). These states are essentially the periodic values in the stable cycles of the quadratic operator's dynamical process. Hence the doubling of the number of discrete states is a direct consequence of period doubling before the onset to

A. Evolution of eigenvalues of weight matrix W



B. Poincare map on r at epoch 4.



C. Poincare map on the evolution of length q_t .

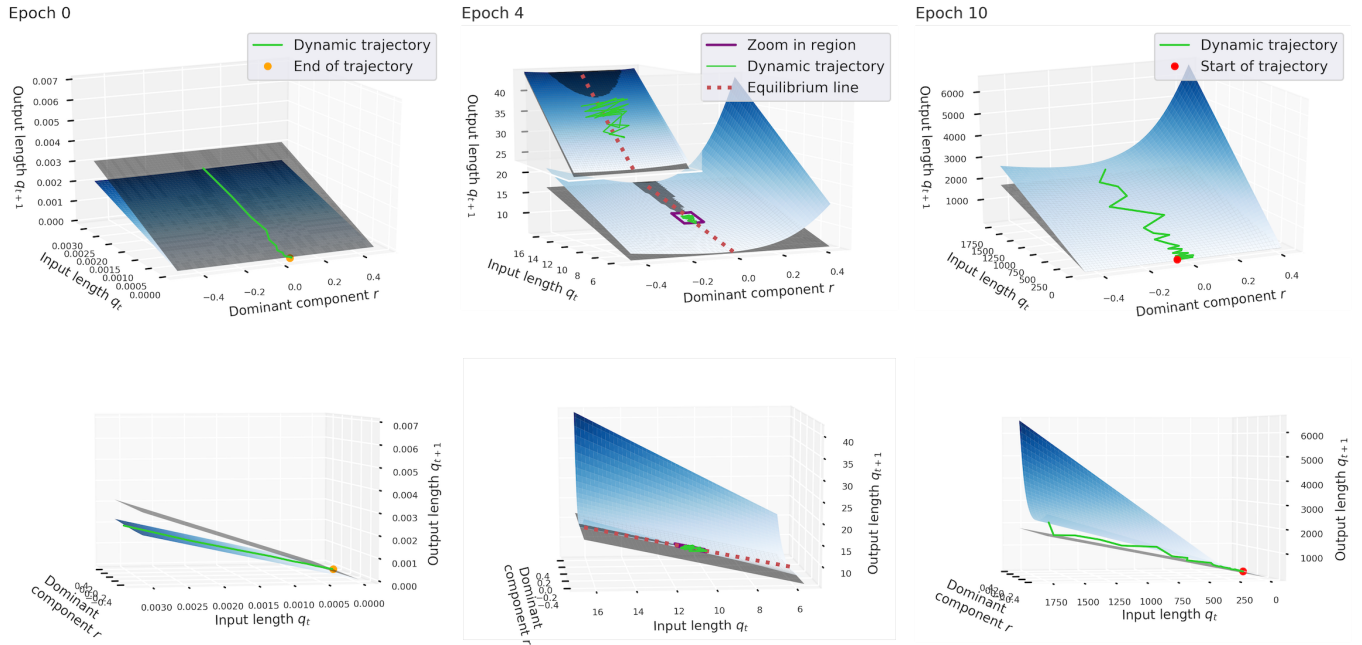


Figure 3: Underlying mechanism of the stability transition in the fully connected layer.

We demonstrate using MLP with single hidden layer for clarity, while more sophisticated models are in figure 9 to 14. (A). At initialization, the eigenvalues of the hidden layer’s weight matrix W are distributed uniformly within a unit circle on the complex plane. As the training proceeds, most eigenvalues evolve towards a broader distribution around 0, while one dominant outlying eigenvalue λ_0 becomes more negative. B. Poincare plot (orange surface) of the dynamics near the edge of chaos. Here $q_t = \|\mathbf{x}_t\|$, and $r_t = \mathbf{x}_t \cdot \mathbf{v}_0 / q_t$ where \mathbf{v}_0 is the eigenvector of the dominant eigenvalue λ_0 . The diagonal grey plane represents $r_{t+1} = r_t$. The orange surface cuts the grey plane at a negative slope, meaning their intersection (red line) is the stable equilibrium line representing $r = r^*$. Indeed the evolution trajectory (green) of an arbitrary initial vector \mathbf{x}_0 oscillates around r^* . C. Poincare plots of q_{t+1} vs. q_t (blue surface) at different viewing angles in different phases. In epoch 0 the network is in a stable state with one trivial equilibrium point $q^* = 0$, at which the green dynamic trajectory of an arbitrary starting \mathbf{x}_0 ends. It then evolves to the chaotic state at epoch 4, when the Poincare surface barely touches the grey diagonal plane representing $q_{t+1} = q_t$, i.e. when equilibrium solutions barely exists. The attractor region (purple box and inset) lies next to the surfaces’ intersection, which are indeed the equilibrium points of the dynamics. At epoch 10, the dynamics become unstable as the two surfaces interchange their relative positions (no stable solutions). Hence the trajectory diverges exponentially while jumping between the two surfaces.

chaos. Maximal number of stable states of the output at the edge of chaos leads to maximal expressivity of the network, therefore making it most optimal. When the system enters the chaotic phase, the output is highly sensitive to small perturbations in input values. Hence despite the high number of states x^{out} can occupy, the network is unable to pass high amount of information from input to the output measured in terms of *effective* mutual information (Methods section) shown in figure 4.

The understanding of model optimality from order-to-chaos transition renders fundamental understandings on model under/over fitting. In our experiments shown in figure 1D, the optimal epoch with the lowest test loss is around epoch 8. Before this epoch the model is in the stable phase, in which the network is able to distinguish some but not all input features due to the limited number of stable states. But since the output states are stable, it is resilient against variations in input data, and hence the features learnt are ‘useful’ features generalizable to test data. After the optimal epoch, the training accuracy increases but not testing accuracy. This is because in the chaotic phase as seen from the logistic map example at $r = 3.7$ in figure 4, the network is highly expressive such that it can match almost any input-output pairs close enough, boosting training accuracy. But the output is very sensitive to tiny variations in inputs as they are not ‘stable’ states. Hence the network does not generalize well to test data. In real problems the network at the exact edge of chaos point has fixed input/output structure, which may not be the best fitting on the data. However expressivity grows exponentially fast as r approaches the edge of chaos, due to the exponentially decreasing bifurcation intervals governed by the first Feigenbaum constant (24). Therefore the best fitting model parameter is going to be very close to the edge of chaos. Overall, it implies that the deep neural network models ‘learn’ by forming numerous **stable** hidden states (features), which are the most abundant near the edge of chaos - a possible generic feature for large composition of non-linear functions yet to be proven.

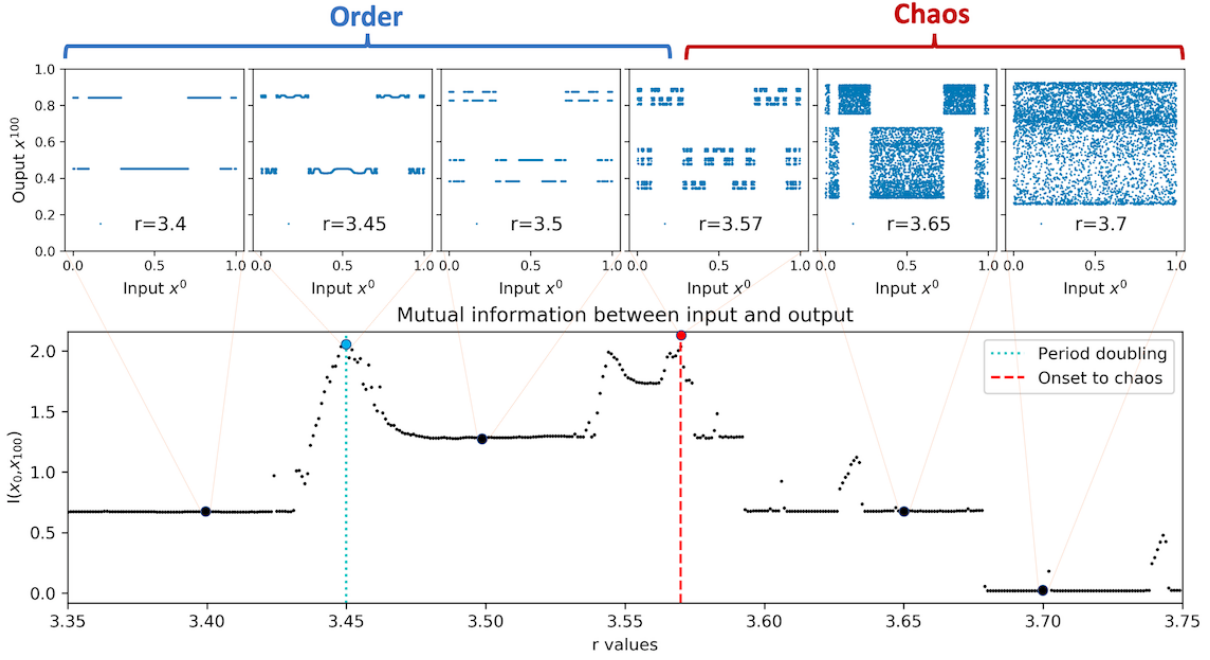


Figure 4: **Pseudo neural network consisting of 100 layers of logistic map** $x^{l+1} = rx^l(1 - x^l)$. Here we denote the input value $x^{in} = x^0$ while the output value $x^{out} = x^{100}$. The bottom figure shows the mutual information $I(x^{in}, x^{out})$ calculated from the top figures at different r values around the transition from order to chaos. When r increases, x^{out} evolves from having 2 states at $r = 3.4$ to 4 states at $r = 3.5$, until it reaches maximum number of states at $r^* \approx 3.57$ at the edge of chaos. Hence the expressivity in terms of the (0th order Renyi) entropy in x^{out} increases with the number of discrete states P approximately as $\ln P$, which leads to higher mutual information. Therefore, maximal mutual information is at the end of period doubling, i.e. onset to chaos r^* . Note that near the period doubling state like $r \approx 3.45$ as shown, x^{out} takes continuous states rather than discrete states, and in turn results in high mutual information $I(x^{in}, x^{out})$. When $r > r^* \approx 3.57$, the network is mostly in chaotic states like $r = 3.65$ and $r = 3.7$. The extremely high sensitivity of x^{out} w.r.t. x^{in} leads to lower effective mutual information, despite the high expressivity in x^{out} . The larger attractor size at $r = 3.7$ than that at $r = 3.65$ leads to lower mutual information as well. Note that although both $r = 3.45$ and $r = 3.57$ are critical phase transition points and have similar mutual information, the later's x^{out} states have more stable states and more spread out. The *effective* mutual information is calculated based on putting each input/output values into 500 uniform bins between 0 and 1 (Methods).

References

1. Miguel A Munoz. Colloquium: Criticality and dynamical scaling in living systems. *Reviews of Modern Physics*, 90(3):031001, 2018.
2. John M. Beggs and Dietmar Plenz. Neuronal avalanches in neocortical circuits. *Journal of Neuroscience*, 23(35):11167–11177, 2003.
3. Daniel Fraiman, Pablo Balenzuela, Jennifer Foss, and Dante R. Chialvo. Ising-like dynamics in large-scale functional brain networks. *Phys. Rev. E*, 79:061922, Jun 2009.
4. P Bak, C Tang, and K Wiesenfeld. Self-organized criticality: an explanation of 1/f noise. *Phys. Rev. Lett*, 59:381, 1987.
5. David P. Feldman, Carl S. McTague, and James P. Crutchfield. The organization of intrinsic computation: Complexity-entropy diagrams and the diversity of natural information processing. *Chaos: An Interdisciplinary Journal of Nonlinear Science*, 18(4):043106, 2008.
6. B.A. Huberman and T. Hogg. Complexity and adaptation. *Physica D: Nonlinear Phenomena*, 22(1):376 – 384, 1986. Proceedings of the Fifth Annual International Conference.
7. Nils Bertschinger and Thomas Natschläger. Real-time computation at the edge of chaos in recurrent neural networks. *Neural computation*, 16(7):1413–1436, 2004.
8. Robert Legenstein and Wolfgang Maass. Edge of chaos and prediction of computational performance for neural circuit models. *Neural Networks*, 20(3):323 – 334, 2007. Echo State Networks and Liquid State Machines.
9. Ben Poole, Subhaneil Lahiri, Maithra Raghu, Jascha Sohl-Dickstein, and Surya Ganguli. Exponential expressivity in deep neural networks through transient chaos. In *Advances in neural information processing systems*, pages 3360–3368, 2016.

10. Jeffrey Pennington, Samuel Schoenholz, and Surya Ganguli. The emergence of spectral universality in deep networks. In Amos Storkey and Fernando Perez-Cruz, editors, *Proceedings of the Twenty-First International Conference on Artificial Intelligence and Statistics*, volume 84 of *Proceedings of Machine Learning Research*, pages 1924–1932, Playa Blanca, Lanzarote, Canary Islands, 09–11 Apr 2018. PMLR.
11. Lechao Xiao, Yasaman Bahri, Jascha Sohl-Dickstein, Samuel Schoenholz, and Jeffrey Pennington. Dynamical isometry and a mean field theory of cnns: How to train 10,000-layer vanilla convolutional neural networks. In *International Conference on Machine Learning*, pages 5389–5398, 2018.
12. John M Beggs and Dietmar Plenz. Neuronal avalanches in neocortical circuits. *Journal of neuroscience*, 23(35):11167–11177, 2003.
13. Clayton Haldeman and John M Beggs. Critical branching captures activity in living neural networks and maximizes the number of metastable states. *Physical review letters*, 94(5):058101, 2005.
14. Diederik P Kingma and Jimmy Ba. Adam: A method for stochastic optimization. *arXiv preprint arXiv:1412.6980*, 2014.
15. Robert M May. Simple mathematical models with very complicated dynamics. *Nature*, 261:459, 1976.
16. Geoff Boeing. Visual analysis of nonlinear dynamical systems: Chaos, fractals, self-similarity and the limits of prediction. *Systems*, 4(4), 2016.
17. Geoffrey E. Hinton, Nitish Srivastava, Alex Krizhevsky, Ilya Sutskever, and Ruslan Salakhutdinov. Improving neural networks by preventing co-adaptation of feature detectors. *CoRR*, abs/1207.0580, 2012.

18. Kaiming He, Xiangyu Zhang, Shaoqing Ren, and Jian Sun. Deep residual learning for image recognition. In *Proceedings of the IEEE conference on computer vision and pattern recognition*, pages 770–778, 2016.
19. Gao Huang, Zhuang Liu, Laurens Van Der Maaten, and Kilian Q Weinberger. Densely connected convolutional networks. In *Proceedings of the IEEE conference on computer vision and pattern recognition*, pages 4700–4708, 2017.
20. Sergey Ioffe and Christian Szegedy. Batch normalization: Accelerating deep network training by reducing internal covariate shift. *CoRR*, abs/1502.03167, 2015.
21. Michael Mahoney and Charles Martin. Traditional and heavy tailed self regularization in neural network models. In Kamalika Chaudhuri and Ruslan Salakhutdinov, editors, *Proceedings of the 36th International Conference on Machine Learning*, volume 97 of *Proceedings of Machine Learning Research*, pages 4284–4293, Long Beach, California, USA, 09–15 Jun 2019. PMLR.
22. Jean Ginibre. Statistical ensembles of complex, quaternion, and real matrices. *Journal of Mathematical Physics*, 6(3):440–449, 1965.
23. CELSO GREBOGI, EDWARD OTT, and JAMES A. YORKE. Chaos, strange attractors, and fractal basin boundaries in nonlinear dynamics. *Science*, 238(4827):632–638, 1987.
24. MJ Feigenbaum. Universality in complex discrete dynamics. Technical report, LA-6816-PR, LASL Theoretical Division Annual Report July 1975September, 1976.

Materials and Methods

Lyapunov exponent estimation

Lyapunov exponent γ characterizes the rate of trajectory separation from perturbed initial conditions, i.e. $|\partial x_t| \approx e^{\gamma t} |\partial x_0|$. The largest or maximal Lyapunov exponent usually dictates the system’s asymptotic behavior, and is commonly used to study the system’s stability. For discrete time dynamics, the maximal Lyapunov exponent can be numerically estimated through iterations:

$$\gamma(x_0) = \lim_{t \rightarrow \infty} \frac{1}{t} \ln \frac{\|x'_t - x_t\|}{\|x'_0 - x_0\|}. \quad (3)$$

Here x'_t and x'_0 are the perturbed final state and initial state respectively: $x'_0 = x_0 + \epsilon$. For simplicity we use the term ‘Lyapunov exponent’ to denote the ‘maximal Lyapunov exponent’.

In our study, the inputs are images which are represented as vectors. We perturb each vector element by adding to it a Gaussian noise of mean 0 and standard deviation 0.0001, i.e. $\epsilon = \mathcal{N}(0, 0.0001)$. The separation is calculated based on the Euclidean distance between the two vectors: $d_t = \|x'_t - x_t\|_2$. Next we apply the dynamic operator $f(x)$ extracted from the neural network repeatedly over 200 times to obtain the convergence of γ . When $\|x'_t - x_t\|$ converges to 0 or diverges to ∞ , the iteration will stop before reaching 200 steps due to numerical limit of the computer. But for $\gamma \approx 0$ such numerical limitation does not show up.

For each model generated throughout the training process, we estimate one γ for each of the 10,000 testing images. Since the Lyapunov exponent depends on the initial vector x_0 , each testing image gives a different γ value. But for each model, these γ values are distributed within a narrow range that exhibits similar stability behaviors as shown in Fig. 5. Therefore for clarity, in the main manuscript we only show the average over 10000 images as the final Lyapunov exponent for each model.

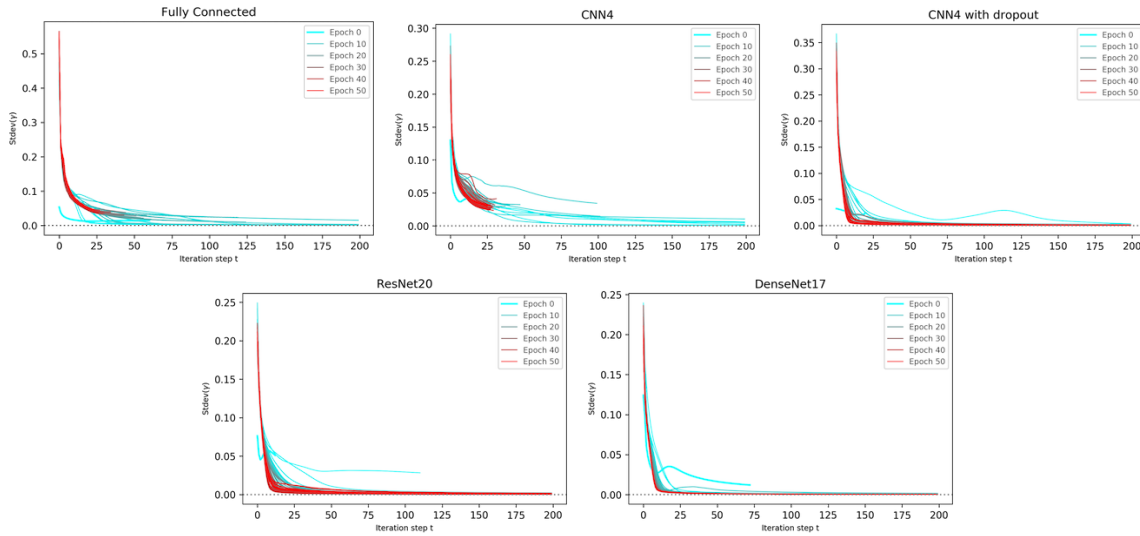


Figure 5: **Standard deviations of Lyapunov exponents over 10000 test images.**

Different Deep Neural Networks

We carry out experiments on various network architectures and training techniques. We used Keras 2.2.4 with Tensorflow backend version 1.13.1. In the training of the networks, we always use ‘adam’ optimizer (14) as it is the most commonly used in computer vision tasks. Learning rate is the default setting in Tensorflow unless otherwise specified. Activation function used throughout is ReLU except for the output layer which is softmax. All of the MLPs are trained on Fashion MNIST dataset as it is simple enough for MLPs to achieve good accuracy. The other models are trained on Cifar10 dataset² which is a standard dataset for sophisticated computer vision models. For MLPs we carried out 10 independent experiments to get the average behaviors. For the other networks, due to the high computational time required for Lyapunov exponent estimation, we only carried out one training process, but the phenomenon of optimality at edge of chaos is universal in each of them.

²<https://www.cs.toronto.edu/~kriz/cifar.html>

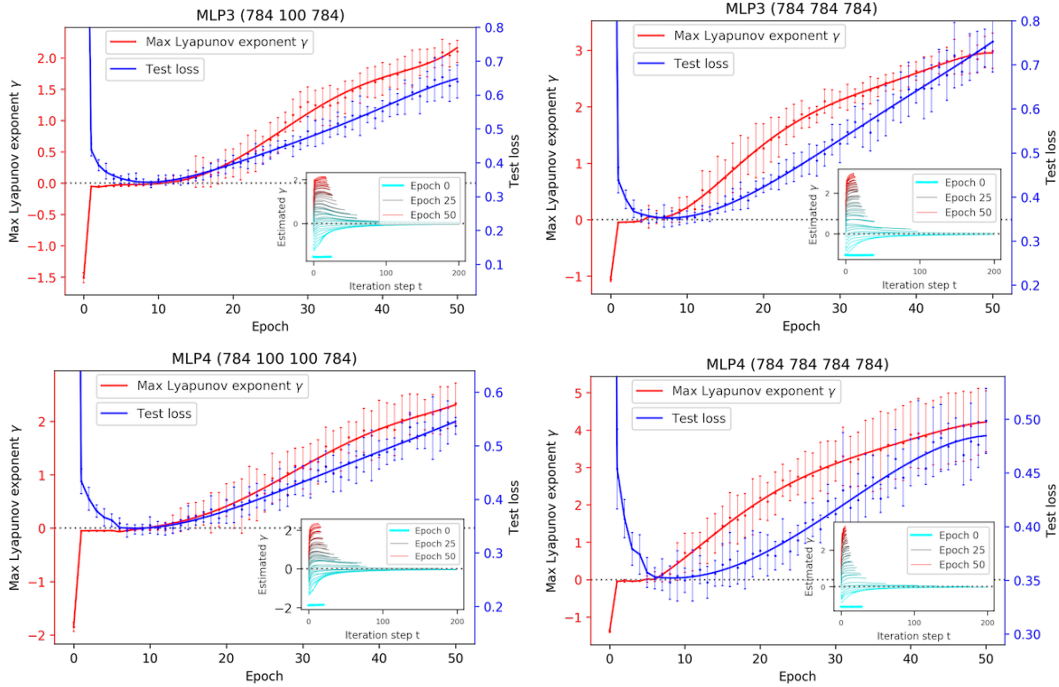


Figure 6: **Lyapunov exponents on various MLPs.** Error bars represent standard error over 10 independent experiments.

Multi-layer perception

The network in figure 1 has 2 hidden layers with 784 nodes each. We also experimented with different versions of MLP that have different number of hidden layers and number of nodes in each layer. Note that the final hidden layer is fixed at 784 nodes - same dimension as the input layer. The models in figure 6 have structure details in their titles. For instance, MLP3 (784 100 784) refers to 3 hidden layers with 784, 100 and 784 nodes each.

Table 1: Test accuracy for MLP.

| | MLP2 | MLP3 (784 100 784) | MLP3 (784 784 784) | MLP4 (784 100 100 784) | MLP4 (784 784 784 784) |
|---------------|------|-----------------------|-----------------------|---------------------------|---------------------------|
| Test Accuracy | 89.7 | 89.8 | 89.8 | 89.8 | 89.9 |

Convolutional networks

We modify the network implementation of the model from keras³. To keep the input-output dimension of the extracted dynamical operator the same, we do not use and pooling layer until after the final convolutional layer. The networks in figure 2A, B and the top two in figure 7 have 5 convolutional layers, with channel sizes (32, 32, 64, 64, 3). Again the layer with 3 channels is to ensure it has the same dimension as input layer. This layer is added to ResNet and DenseNet as well for the same reason. After the convolutions we add a MaxPooling2D layer to shrink the size by 2X2, followed by a dense layer of 512. For the models in figure 11-14, the pooling layer has kernel size 3X3 and the next dense layer has dimension 300, such that the dense layer has the same dimension as the output from the pooling layer. For the networks with dropout layers, the dropout layer (drop ratio 0.25) is added after every 2 convolutional layers and after the resizing convolutional layer with channel size 3, and one more (drop ratio 0.5) after the dense layer.

Table 2: Test accuracy for CNN.

| | CNN4 | CNN4 w. dropout | CNN8 | CNN8 w. he_normal | CNN8 w. dropout |
|---------------|------|--------------------|------|----------------------|--------------------|
| Test Accuracy | 64.0 | 71.5 | 60.2 | 61.2 | 66.7 |

Residual networks and Densenet

For ResNet, we modify the network implementation from keras⁴ for both 20, 56 and 110 layers ResNet. Again we do not put any pooling layer until after the final convolutional layer. For longer training epochs in figure 8, we reduce the default learning rate by 10 times at epoch 80 to improve accuracy. Note that there is no dropout layer in our ResNet models, such that

³https://keras.io/examples/cifar10_cnn/

⁴https://keras.io/examples/cifar10_resnet/

we could isolate the dropout layer’s effect from the experiments. For DenseNet, we adopt the simple implementation from TheAILearner⁵. DenseNet3x4 has 3 blocks of 4 layers each, and DenseNet4x6 has 4 blocks of 6 layers each. Both have no pooling in the transition block. The final global pooling layer is replaced with a maxpooling layer, as our final convolutional layer has only 3 channels which are too few for global pooling to work.

Table 3: Test accuracy for CNN.

| | ResNet20 | ResNet56 | ResNet110 | DenseNet3x4 no Aug or last dropout | DenseNet3x4 | DenseNet4x6 |
|---------------|----------|----------|-----------|--|-------------|-------------|
| Test Accuracy | 78.8 | 88.6 | 86.0 | 75.7 | 78.5 | 87.6 |

Effective mutual information

Mutual information (MI) measure $I(x^{in}, x^{out})$ is commonly used to study neural networks. The mutual information can be decomposed into:

$$I(x^{in}, x^{out}) = H(x^{out}) - H(x^{out}|x^{in}). \quad (4)$$

For deterministic functions that maps x^{in} to x^{out} , the second term on the right is theoretically 0. But in chaotic phase this can only be true with perfect accuracy on the value of x^{in} , which is impossible in practice. Therefore, we numerically measure $I(x^{in}, x^{out})$ by putting them into 500 bins of size 0.002, which is similar to a measurement error of 0.002. Note that both x^{in} and x^{out} are confined in the range (0, 1). To ensure accurate statistics, we sample 4,000,000 pairs of (x^{in}, x^{out}) uniformly in the range $0 < x^{in} < 1$, such that each bin has at least 16 samples.

Because the mapping from input to output is deterministic, $H(x^{out}|x^{in}) = 0$ in the order phase. Therefore $H(x^{out})$ represents the expressivity of the logistic map neural network $f_r(x)$.

⁵<https://github.com/TheAILearner/DenselyConnectedConvolutional-Networks>

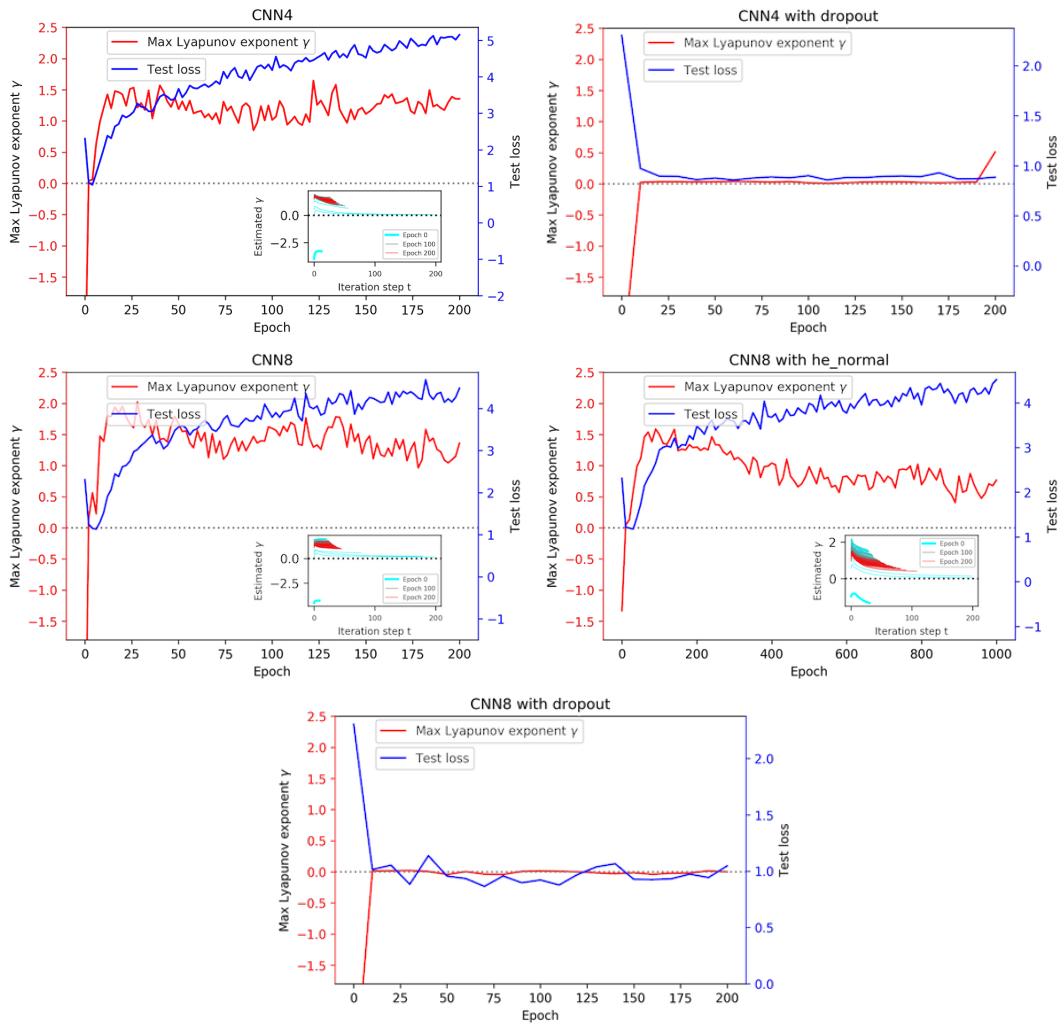


Figure 7: Lyapunov exponents on various CNNs.

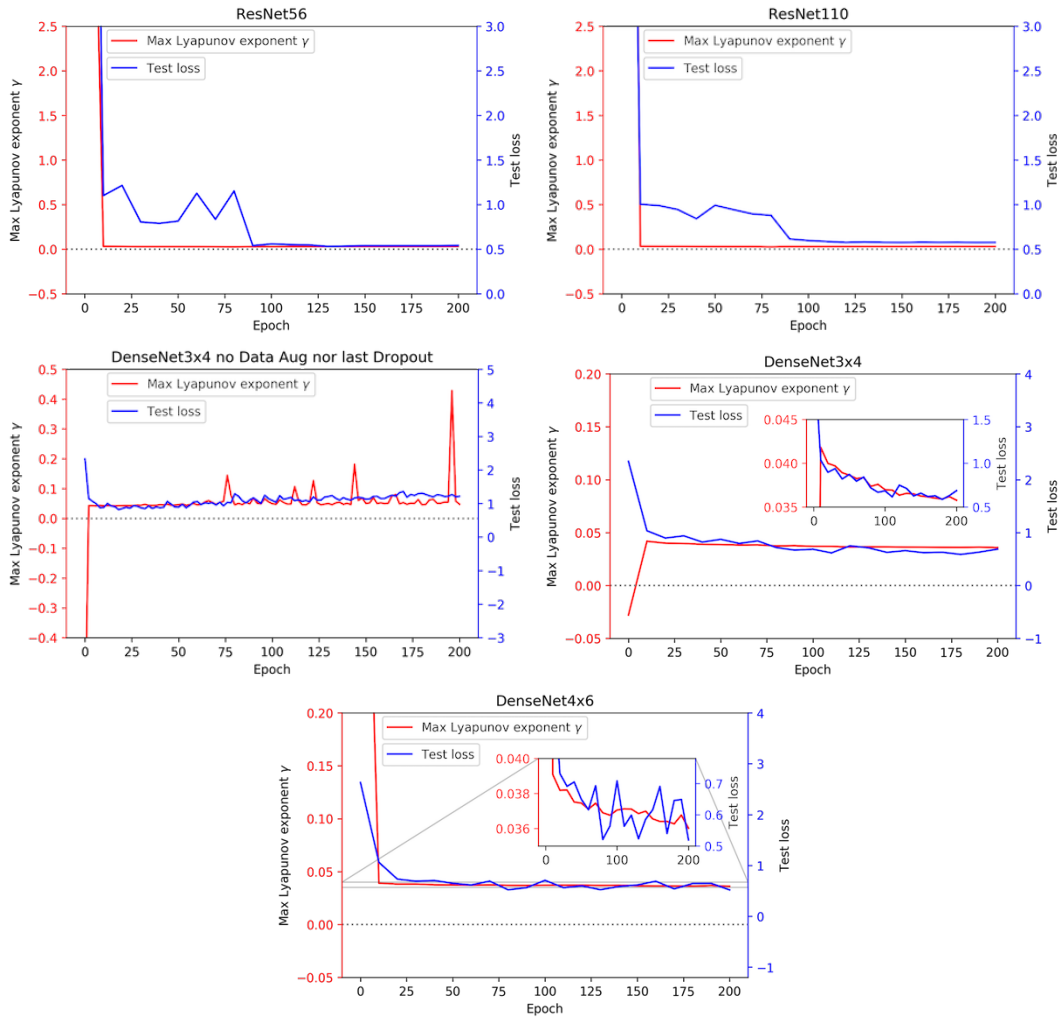


Figure 8: Lyapunov exponents on various ResNets and DenseNets.

It is known that in the order phase before reaching the first onset to chaos at $r \approx 3.57$, the logistic map $g_r(x)$ converges to a stable cycle of period P for any input x . As $f_r(x)$ is 100 compositions of $g_r(x)$, it is reaching the asymptotic behavior of P -period cycle, such that x^{out} converges towards the P different periodic values. In other words, x^{out} values are concentrated in only P different discrete states, as seen in Fig. 4 for $r < 3.57$. Therefore the effective mutual information is equivalent to the entropy from those P states, i.e. $I(x^{in}, x^{out}) = H(x^{out}) \approx \ln P$ if we use the 0th order Renyi entropy for analytical simplicity. This implies that the expressivity of $f_r(x)$ is maximal when P is maximal. Since P is maximal at the end of period doubling, i.e. onset to chaos at $r \approx 3.57$, we expect the mutual information peaks at this point, which is indeed the case shown in Fig. 4.

However, in the chaotic phase, the assumption that $H(x^{out}|x^{in}) = 0$ fails in practice, because an infinitesimally small difference in the input x^{in} will result in huge difference in x^{out} . In this case $H(x^{out}|x^{in}) > 0$, so that $I(x^{in}, x^{out}) < H(x^{out})$, and the expressivity of the network decreases from the onset to chaos $r \approx 3.57$.

Another interesting finding in the mutual information of $f_r(x)$ is that $I(x^{in}, x^{out})$ is locally maximal at the point of period doubling, $r = 3.45$ as shown in Fig. 4 for instance. This is because at those critical points separating two different stable states, x^{out} do not only converge to their stable equilibrium values, but a considerable portion exists between the two pairs of stable equilibriums as shown in Fig. 4 for $r = 3.45$. Such intermediate states contributes significantly to the mutual information. In other words, the convergence to asymptotic stable points fails to happen at the period doubling critical points, resulting in diverse states. However, these states between the stable states are sensitive to perturbations, and not as useful in practice.

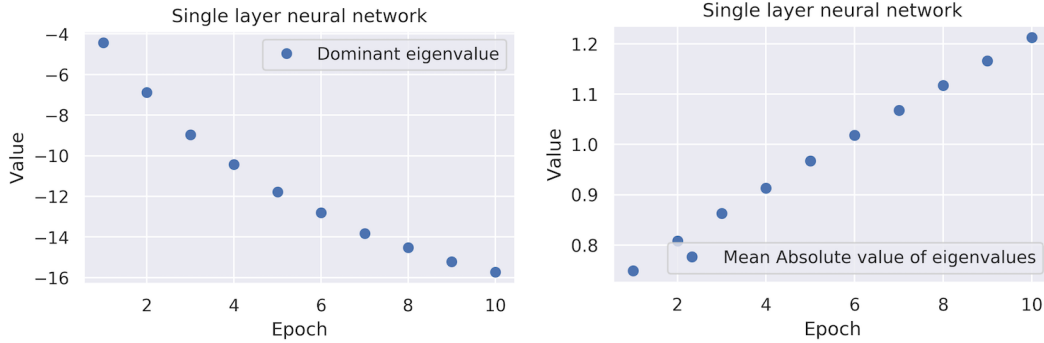


Figure 9: **Evolution of the eigenvalues in the single layer fully connected networks.**

Eigenvalue evolution for different networks

For the networks other than MLP, we design the second last layer to be a fully connected layer with same dimension as the previous layer. For all of the networks tested, the same qualitative pattern of evolution described in the main text is found, with the exception of the second hidden layer of the 2-hidden layer MLP. But in this case, the first hidden layer carried the universal evolution pattern. For the Poincare plot in figure 3C, we choose a random test image and starts to evolve it using the dynamical operator. For visual clarity we discard the first 20 iterations as the process was still trying to settle down onto the Poincare surface. Since the input vector at the 20th time step of evolution settles close to the equilibrium line $r_0 = r^*$, The Poincare surface is calculated based on the vector x_{20} . We vary both length and dominant component ratio r_0 from x_{20} to map out the 2D Poincare surface.

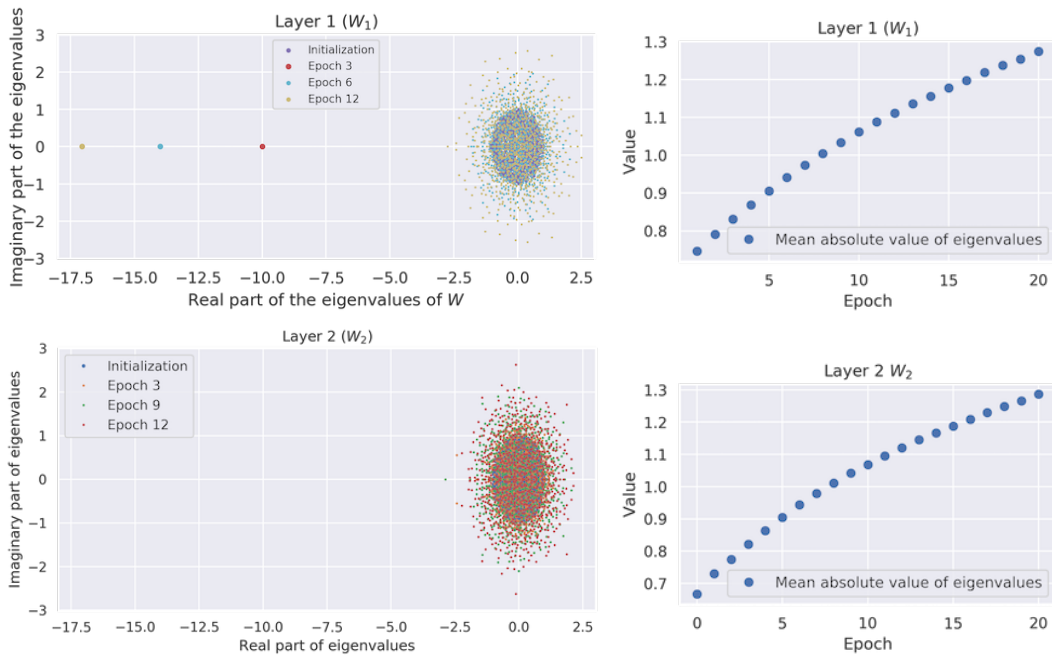


Figure 10: Evolution of the eigenvalues in the 2-hidden-layer fully connected network.

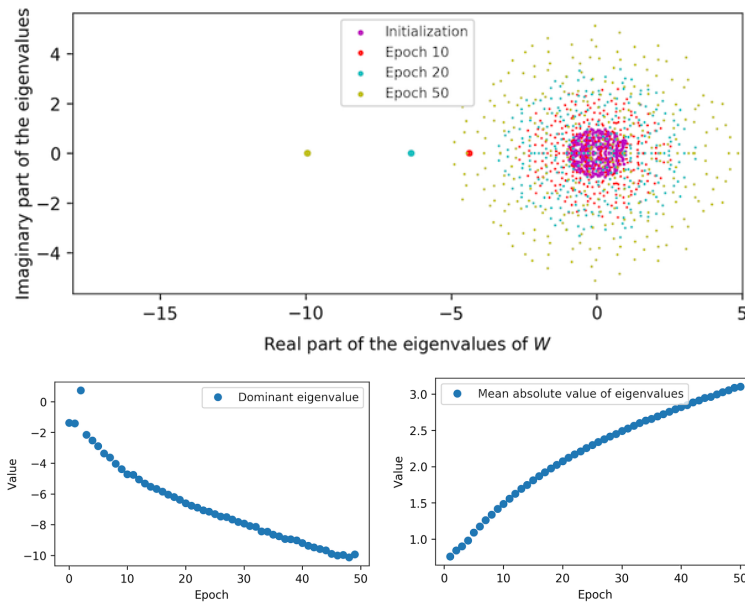


Figure 11: Evolution of the eigenvalues in the fully connected layer of CNN. The network has 5 convolutional layers and 1 fully connected layer with size 300X300.

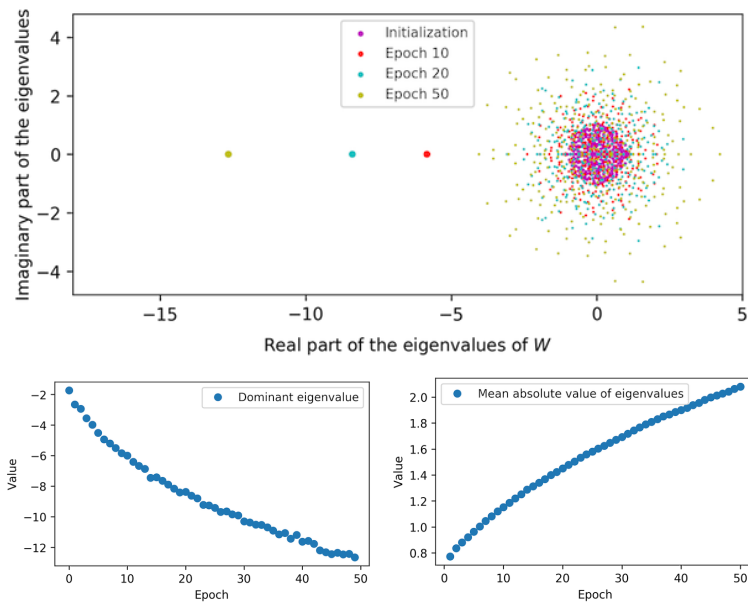


Figure 12: **Evolution of the eigenvalues in the fully connected layer of CNN with dropout layers.** The network has 5 convolutional layers and 1 fully connected layer with size 300X300.

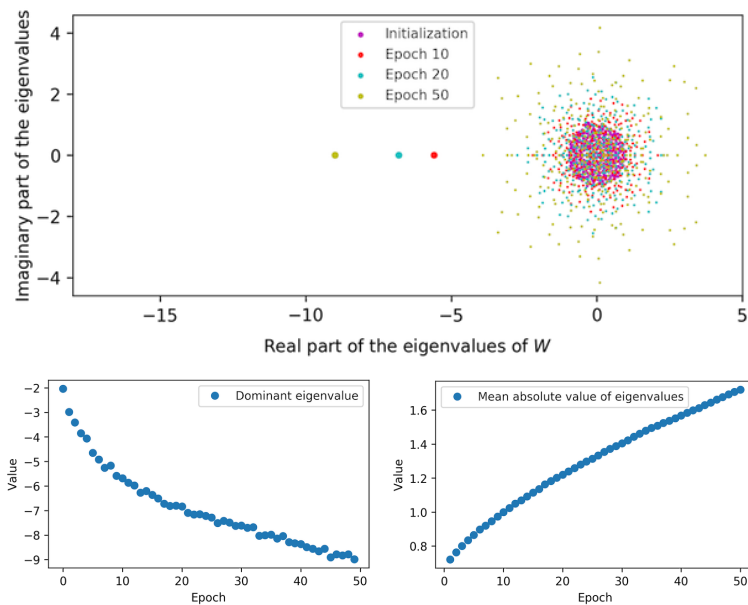


Figure 13: **Evolution of the eigenvalues in the fully connected layer of ResNet.** The network has 20 convolutional layers and 1 fully connected layer with size 300X300.

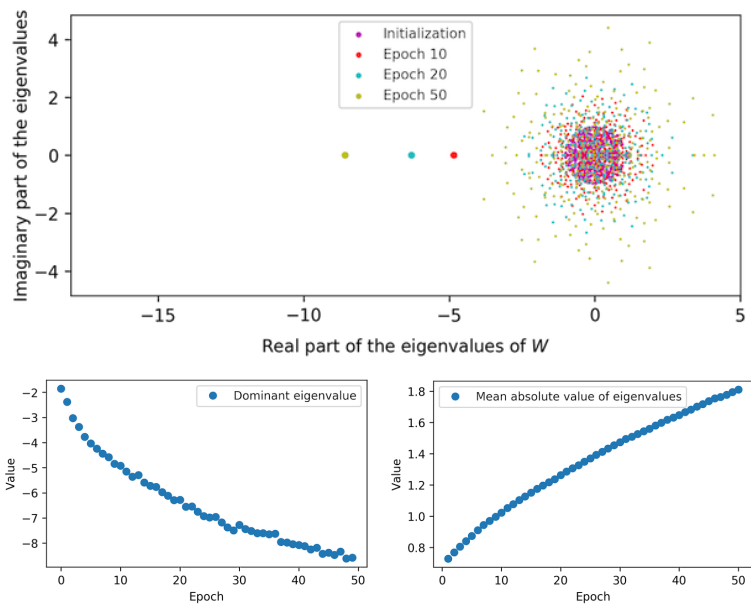


Figure 14: **Evolution of the eigenvalues in the fully connected layer of DenseNet.** The network has 17 convolutional layers and 1 fully connected layer with size 300X300.